P H Y S I C A L R E V I E W L E T T E R S

Kinetic Model for Sheared Granular Flows in the High Knudsen Number Limit

V. Kumaran

Department of Chemical Engineering, Indian Institute of Science, Bangalore 560 012, India

The sheared granular flow of rough inelastic granular disks is analyzed in the high Knudsen number limit, where the frequency of particle-wall collisions is large compared with particle-particle collisions, using a kinetic theory approach. An asymptotic expansion is used in the small parameter $\varepsilon = (n\sigma L)$, which is the ratio of the frequencies of particle-particle and particle-wall collisions, where n is the number of disks per unit area, σ is the disk diameter, and L is the channel width. The collisions are specified using a normal coefficient of restitution e_n and a tangential coefficient of restitution e_t. The analysis identifies two regions in the $e_t - e_n$ parameter space, one where the final steady state is a static one in which the translational velocities of all particles decrease to zero, and the second where the final steady state is a dynamic one in which the mean square velocities scale as a power of ε in the limit $\varepsilon \to 0$. Both of these predictions are shown to be in quantitative agreement with computer simulations.

Rapid flows of granular material have been analyzed using methods from the kinetic theory for dense gases. These include approximate approaches that modified the Navier-Stokes mass, momentum, and energy equations by adding a dissipation term due to inelastic collisions in the energy equation [1–4], as well as asymptotic approaches that used an expansion in the inelasticity and the Knudsen number [5–7]. These have proved to be quite successful [8] in the low Knudsen number limit, where the mean free path is small compared to the macroscopic length scale. However, there are many practical situations, such as the chute flows and flow in thin layers, where the distance between boundaries could be of the order of a few particle diameters, and it is important to examine whether a kinetic theory approach can be fruitfully employed for high Knudsen number flows. It is also of interest to examine whether the rheology is sensitive to the nature of the particle-wall interaction. One approach is to try and determine the distribution function and constitutive relations in the opposite high Knudsen number regime, where the frequency of particle-wall interactions is large compared to particle-particle interactions. This is difficult, in general, because the distribution function is sensitive to the nature of the particle-wall interactions, and it may not be possible to obtain analytical results in all cases. Analytical results were obtained for the velocity distribution function for smooth particles by Kumaran [9] using an asymptotic analysis in the small parameter $\varepsilon = n\sigma L$, which is proportional to the inverse of the Knudsen number, where n is the number density, σ is the diameter of the particle, and L is the channel width. The disadvantage of that study was that it was restricted to smooth particles where the angular momentum of the particles was not incorporated in the description, though the particle-wall collision rule did permit the transport of momentum from the wall to the particle in the tangential direction. The present study provides the results for rough particle-wall interactions where

the transfer of momentum parallel and perpendicular to the surface at contact is incorporated. These two models are the most general models for particle interactions with a flat wall, even though it is possible to formulate more detailed models that incorporate sticking and sliding friction in collisions. Therefore, these provide the range of scaling laws for the stresses in a high Knudsen number flow bounded by flat walls. However, these results are not expected to hold for more complicated models, such as the bumpy wall model.

The configuration and coordinate system used in the analysis is shown in Fig. 1. The model predictions were compared with simulations carried out using the hard disk event driven simulation technique [10]. The simulation cell typically consisted of 125 particles, and a total of 40 periodic images of the simulation cell were used in the lateral "flow" direction. This large number of periodic images was necessary since there are particles that travel nearly parallel to the wall, and they undergo very infrequent collisions in the dilute limit.
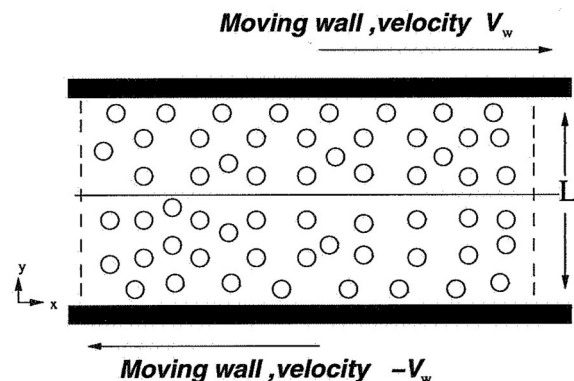

FIG. 1. Schematic of two-dimensional rough disks sheared with two parallel moving rough walls.

We use the collision rules for rough, inelastic hard spheres, formulated by Lun [4], which is a modification of the collision rules of Bryan [11] for perfectly rough perfectly elastic spheres. Consider a collision between two particles with precollisional linear velocities $\mathbf{u}$ and $\mathbf{u}^*$ and angular velocities ω and ω^*, such that the unit vector along the line joining the centers of the particles is $\mathbf{k}$. The precollisional relative velocity at the point of contact is $\mathbf{g} = [\mathbf{u} + (\sigma\mathbf{k}/2) \times \omega] - [\mathbf{u}^* - (\sigma\mathbf{k}/2) \times \omega^*]$. The collision rules stipulate that the postcollisional relative velocity at the point of contact $\mathbf{g}'$ is related to the precollisional relative velocity $\mathbf{g}$ by

$$g'_n = -e_n g_n, \qquad g'_t = -e_t g_t, \qquad (1)$$

where g_n and g'_n are the components of $\mathbf{g}$ in the direction of $\mathbf{k}$, g'_t and g_t are the components of $\mathbf{g}$ perpendicular to the direction of $\mathbf{k}$, and e_n and e_t are the normal and tangential coefficients of restitution.

In the absence of binary collisions, a steady state is achieved if the particle velocity distribution is recovered after two wall collisions. In the present case, we show by analyzing the evolution of a particle velocity due to wall collisions that the steady state distribution is a delta function at the location in velocity space where the translational velocities are equal to zero, and the rotational velocity is equal to the ratio of the wall velocity and the particle diameter. If the particle collides with the wall at $y = -L/2$, the particle velocity after collision derived using Eq. (1) as indicated in Lun [4] is

$$u'_x = (1 - 2\eta_2)u_x - 2\eta_2\left(V_w + \frac{\sigma}{2}\omega\right),$$

$$u'_y = (1 - 2\eta_1)u_y, \qquad (2)$$

$$\omega' = \omega - \frac{4\eta_2}{\kappa\sigma}u_x - \frac{4\eta_2}{\kappa\sigma}\left(V_w + \frac{\sigma}{2}\omega\right),$$

where subscripts x and y stand for flow and gradient directions, respectively, $\eta_2 = \frac{(1+e_t)}{2}\frac{\kappa}{1+\kappa}$, $\eta_1 = \frac{1+e_n}{2}$, and $\kappa = (4I/m\sigma^2)$, where I is the moment of inertia. The velocity after a subsequent collision with the wall at $y = L/2$, (u''_x, u''_y, ω''), is related in a similar manner to (u'_x, u'_y, ω'). If the velocity of particle after two successive collisions is the same as the initial velocity, $u''_x = u_x$, $u''_y = u_y$ and $\omega'' = \omega$. The solution for the velocity of the particle at steady state is

$$u'_x = u_x = 0, \qquad u'_y = u_y = 0, \qquad \omega' = \omega = \frac{-2V_w}{\sigma}. \qquad (3)$$

The above results indicate that at steady state the distribution function is a delta function at the location in velocity space where the flow and gradient directional velocities are zero, and the rotational velocity distribution is $\frac{-V_w}{\sigma/2}$.

Next, we consider the evolution of a particle whose velocity is different from those in Eq. (3). For this purpose,

we define the deviation from the steady state angular velocity as $\Omega = (\omega + 2V_w/\sigma)$. Considering two wall collisions as one event, the velocity and angular velocity after $(i + 1)$ pairs of wall events are related to those after i pairs of wall collisions by

$$\begin{pmatrix} u_x^{(i+1)} \\ \sigma\Omega^{(i+1)} \end{pmatrix} = A\begin{pmatrix} u_x^{(i)} \\ \sigma\Omega^{(i)} \end{pmatrix}, \qquad (4)$$

where

$$A = \begin{pmatrix} [(1 - 2\eta_2)^2 - 4\eta_2^2/\kappa] & (2\eta_2^2(1 - \kappa)/\kappa) \\ \frac{-8\eta_2^2(1-\kappa)}{\kappa^2} & [(1 - 2\eta_2/\kappa)^2 - 4\eta_2^2/\kappa] \end{pmatrix} \qquad (5)$$

and η_1 and η_2 are provided after Eq. (2). The magnitude of the largest eigenvalue $\lambda_{x\Omega}$ of the transfer matrix A determines the rate of decrease of the velocity u_x with number of pairs of collisions. For disks of uniform density, $\kappa = (1/2)$, and there are two complex conjugate eigenvalues for A when $e_t > 0.0294373$. It is found that for $e_t > 0.0294373$, both the eigenvalues are real. However, in all cases, the magnitude of the eigenvalues is less than 1 for $|e_t| < 1$. The cross stream velocity after a pair of wall collisions, $u_y^{(i+1)}$, is related to the cross stream velocity before a pair of collisions, by

$$u_y^{i+1} = \lambda_y u_y^i, \qquad (6)$$

where $\lambda_y = e_n^2$. Since the magnitudes of the eigenvalues $\lambda_{x\Omega}$ and λ_y are always less than 1, the particle velocities converge to the steady state values given by Eq. (3) independent of the initial velocities.

In the presence of binary collisions, there are two possible final steady states. One is the state where all particle velocities decrease to zero at long times, because the frequency of wall-particle collisions, which tends to reduce the translational velocity, is larger than that of interparticle collisions. The frequency of wall-particle collisions per unit area is proportional (nu_y/L), whereas the number of interparticle collisions is proportional to $n^2\sigma(u_x^2 + u_y^2)^{1/2}$. The ratio of the binary collision frequency and the particle-wall collision frequency is given by $[n\sigma L(u_x^2 + u_y^2)^{1/2}/u_y]$. Since we are considering the limit $(n\sigma L) = \varepsilon \ll 1$, the ratio of binary and particle-wall collisions is always small if u_x decreases to zero faster than u_y as the particle undergoes wall collisions. Therefore, it is expected that the final steady state will be one in which the translational velocities of the particles reduce to zero if u_x reduces to zero faster than u_y as the particle undergoes wall collisions. In the opposite case, where u_y reduces to zero faster than u_x as the particle collides with the wall, it is expected that $[(u_x^2 + u_y^2)/u_y]$ will increase with the number of collisions, and this ratio could be large enough that $[n\sigma L(u_x^2 + u_y^2)^{1/2}/u_y]$ will be $O(1)$ even though $n\sigma L$ is small.

Thus, the ratio $(\lambda_{x\Omega}/\lambda_y)$ provides the relative rate of decrease of u_x and u_y with a number of pairs of wall collisions. For $\lambda_{x\Omega} < \lambda_y$, u_x decreases to zero faster than u_y and the translational energy goes to zero at long time. For $\lambda_{x\Omega} > \lambda_y$, the system reaches a steady state, where the average translational energy of the system is constant. The above predictions are in good agreement with the results of simulations. In the results presented here, we assume that the coefficients of restitution for particle-particle and particle-wall collisions are equal. Figure 2 shows the boundary between the parameter regimes for the zero translational energy steady state, and the nonzero translational energy steady state. The points are the parameter values for which simulations were carried out on either side of the boundary, and the pluses are the points at which the final steady state had zero translational energy, while the circles are the points at which the final steady state had nonzero energy.

The physical picture of the evolution of the particle velocity in the dynamical steady states is as follows. For particles that have just undergone a collision, the frequency of wall-particle collisions is large compared to that of binary collisions. The particle undergoes collisions with the wall, and the velocity evolves according to

$$u_x^{(i)} = \lambda_{x\Omega} u_x^{(i-1)} = \lambda_{x\Omega}^i u_x^{(0)}, \qquad u_y^{(i)} = \lambda_y u_y^{(i-1)} = \lambda_y^i u_y^{(0)},$$
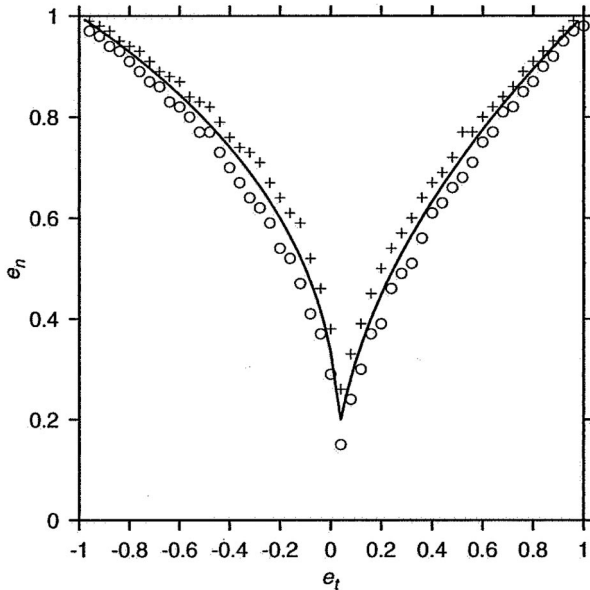$$\Omega^{(i)} = \lambda_{x\Omega} \Omega^{(i)} = \lambda_{x\Omega}^i \Omega^{(0)}, \qquad (7)$$

FIG. 2. Static and dynamic regions for different values of e_t and e_n and $\kappa = 0.5$. The analysis predicts that dynamical steady states will be observed below the solid line, and static steady states above the solid line. The circles are points at which dynamical steady states were observed in simulations, and the pluses are points where static steady states were observed in simulations.

where i is the number of pairs of particle-wall collisions after the most recent binary collision. As the number of wall collisions increases, the frequency of binary collisions becomes equal to that of wall-particle collisions for $(u_x/u_y) \sim \varepsilon^{-1}$, or $i = i_m \sim [\log(\varepsilon)/\log(\lambda_y/\lambda_{x\Omega})]$. At this point, the particle undergoes a binary collision that scatters the velocity. This cycle repeats itself, and a dynamical steady state is achieved. It is convenient to separate the distribution function $f(u_x, u_y, \Omega) = \Sigma_i f_i(u_x, u_y, \Omega)$, where the index i represents the number of pairs of wall collisions after the most recent binary collision. The relation between f_i and f_{i-1} at steady state can be inferred from the condition that the frequency of wall collisions of particles with index $i-1$, which results in an accumulation of particles with index i, is equal to the frequency of wall collisions of particles with index i, which results in a depletion of particles with index i (note that the frequency of binary collisions is small compared to that of wall collisions for $i < i_m$). Since the wall flux of particles with velocity $u_y^{(i)}$ is equal to $nu_y^{(i)} f_i$, the flux balance provides a relation for f_i in terms of f_{i-1},

$$f_i = \lambda_y^{-1} f_{i-1} = \lambda_y^{-i} f_0. \qquad (8)$$

Equation (8) relates f_i to f_0, but does not provide the dependence of f_0 on ε. This dependence is estimated from the normalization condition, which requires that the sum of f_i over all i is $O(1)$. The upper limit in the summation can be estimated as the number of collisions at which the frequency of binary and wall-particle collisions become equal $i = i_m$, since the distribution function decreases as the number of wall collisions increases beyond this point. Therefore, the normalization condition is satisfied only if $f_0 \sim \lambda_y^{i_m}$, or

$$f_0 \sim \varepsilon^{[\log(\lambda_y)/\log(\lambda_y/\lambda_{x\Omega})]}, \qquad (9)$$

since $i_m = [\log(\varepsilon)/\log(\lambda_y/\lambda_{x\Omega})]$. A more exact kinetic theory calculation would require the specification of the functional dependence of f_0 on θ in Eq. (8) by a self-consistent calculation, so that the distribution function is completely specified. However, we do not carry out this calculation, since it is not required for obtaining the scaling laws for the stresses.

The moments of the velocity distribution can now be determined as

$$\langle \mathbf{u}\mathbf{u} \rangle \sim \int d\theta \sum_{i=0}^{i_m} (\mathbf{u}^{(i)}\mathbf{u}^{(i)}) f_i(\theta). \qquad (10)$$

The following scaling of the moments of the distributions with ε are evaluated analytically using (7) for $u_x^{(i)}$ and $u_y^{(i)}$,

TABLE I. A comparison of the theoretical and simulation results for the scaling laws for the velocity moments with ε. The theoretical results are from Eq. (11), while the simulation results are obtained by fitting the simulation results in the interval $0.008 \leq \varepsilon \leq 0.08$ to a power law, and extracting the exponent.

e_t	e_n	$\frac{\log(\langle u_x^2 \rangle)}{\log(\varepsilon)}$		$\frac{\log(\langle u_y^2 \rangle)}{\log(\varepsilon)}$		$\frac{\log(-\langle u_x u_y \rangle)}{\log(\varepsilon)}$	
		Theor.	Simu.	Theor.	Simu.	Theor.	Simu.
0.60	0.65	2.5074	2.4865	2.5074	2.5261	2.5074	2.5696
0.70	0.75	2.6310	2.5944	2.6310	2.6285	2.6310	2.6583
0.80	0.85	3.1899	2.9858	3.1899	3.0050	3.1899	3.0736
0.70	0.70	2.0000*	1.7839	2.0000	1.9956	2.0000	2.0338
0.80	0.80	2.0000*	1.7559	2.0000	1.9869	2.0000	2.0245
0.90	0.90	2.0000*	1.6834	2.0000	1.9739	2.0000	2.0126
0.65	0.60	1.4581	1.4437	1.7291	1.7306	1.7291	1.7204
0.75	0.70	1.3516	1.3218	1.6758	1.7050	1.6758	1.6913
0.85	0.80	1.1453	1.1550	1.5727	1.5653	1.5727	1.5807

(8) for f_i, and (9) for f_0:

$$\langle u_x^2 \rangle \sim \varepsilon^{[\log(\lambda_y)/\log(\lambda_y/\lambda_{x\Omega})]} \quad \text{for } (\lambda_{x\Omega}^2/\lambda_y) < 1,$$

$$\sim \varepsilon^{[2\log(\lambda_{x\Omega})/\log(\lambda_y/\lambda_{x\Omega})]} \quad \text{for } (\lambda_{x\Omega}^2/\lambda_y) > 1,$$

$$\sim \varepsilon^2 \frac{\log(\varepsilon)}{\log(\lambda_y/\lambda_{x\Omega})} \quad \text{for } (\lambda_{x\Omega}^2/\lambda_y) = 1, \qquad (11)$$

$$\langle u_x u_y \rangle \sim \varepsilon^{[\log(\lambda_y)/\log(\lambda_y/\lambda_{x\Omega})]},$$

$$\langle u_y^2 \rangle \sim \varepsilon^{[\log(\lambda_y)/\log(\lambda_y/\lambda_{x\Omega})]}.$$

The moments of the distribution function obtained from simulations were found to be well fitted by a power law form for low ε. The deviation of the simulation results from the power law fit was found to be less than 1% of the value of the velocity moment for $\varepsilon \leq 0.1$ for all values of the coefficient of restitution, except for $e_t = e_n(\lambda_{x\Omega} = \lambda_y^2)$, for which the theoretical prediction (11) had a logarithmic correction. The power law exponents obtained from the simulations in the range $0.008 \leq \varepsilon \leq 0.08$ are compared with the theoretical predictions in Table I. It is observed that there is excellent agreement between the theoretical predictions and the simulation results in most cases. One exception is the results for $\langle u_x^2 \rangle$ for $e_t = e_n$ (or $\lambda_{x\Omega} = \lambda_y^2$). In this case, the theoretical prediction (11) has a logarithmic correction $\langle u_x^2 \rangle \sim \varepsilon^2 \log(\varepsilon)$, which is not incorporated while determining the scaling from the simulation, resulting in relatively poor agreement. The other exception is the result for $e_t = 0.80$ and $e_n = 0.85$, where the theoretically predicted slope is large, and the range of ε studied in the simulations is not sufficient to obtain convergence to the theoretically predicted scaling law. For all

other values, there is excellent agreement between the theoretical predictions and the simulation results.

Thus, the present analysis establishes that the kinetic theory approach can be employed to model the rheology in the high Knudsen number limit for rough particles. The predictions of the model are in quantitative agreement with the results of simulations, both for the regimes of static and dynamic steady states and for the velocity moments or stresses in the dynamic steady state. The implications of the analysis for the rheology of high Knudsen number flows are as follows. The shear stress exerted on the top and bottom surfaces, scaled by the particle mass, is proportional to $n V_w^2 \varepsilon^{[\log(\lambda_y)/\log(\lambda_y/\lambda_{x\Omega})]}$, where V_w is the wall velocity. Consequently, the shear stress scales as the square of the wall velocity in this limit, and the stress-strain relationship is represented by the "Bagnold law" $\sigma_{ij} = B_{ij}(V_w/L)^2$, where σ_{ij} are the components of the stress tensor and (V_w/L) is the mean strain rate. The "Bagnold coefficient" B_{xy} is proportional to $(nL^2)\varepsilon^{[\log(\lambda_y)/\log(\lambda_{x\Omega}/\lambda_y)]}$. The Bagnold coefficient for the normal stress in the cross stream direction, B_{yy}, is also proportional to $(nL^2)\varepsilon^{[\log(\lambda_y)/\log(\lambda_{x\Omega}/\lambda_y)]}$. The Bagnold coefficient for the normal stress in the streamwise direction B_{xx} depends on the value of $(\lambda_{x\Omega}^2/\lambda_y)$, but it is proportional to (nL^2) times a power of ε. This indicates that the Bagnold coefficient is very different in the high Knudsen number regime than it is in the low Knudsen number regime, and provides the explicit dependence of the Bagnold coefficient on the channel width. Though the present results are restricted to the case where gravity is ignored and the walls are considered to be flat, they provide some indication of the variation of the Bagnold constant with Knudsen number for rapid flows in the high Knudsen number limit.

[1] S. B. Savage and D. J. Jeffrey, J. Fluid Mech. **110**, 255 (1981).
[2] J. T. Jenkins and S. B. Savage, J. Fluid Mech. **130**, 187 (1983).
[3] J. T. Jenkins and M. W. Richman, J. Fluid Mech. **171**, 53 (1986).
[4] C. K. K. Lun, J. Fluid Mech. **233**, 539 (1991).
[5] N. Sela and I. Goldhirsch, J. Fluid Mech. **361**, 41 (1998).
[6] J. J. Brey, J. W. Dufty, C.-S. Kim, and A. Santos, Phys. Rev. E **58**, 4638 (1998).
[7] V. Kumaran, J. Fluid Mech. **506**, 1 (2004).
[8] I. Goldhirsch, Annu. Rev. Fluid Mech. **35**, 267 (2003).
[9] V. Kumaran, J. Fluid Mech. **340**, 319 (1997).
[10] M. Bose and V. Kumaran, Phys. Rev. E **69**, 061301 (2004).
[11] G. H. Bryan, Rep. Br. Ass. Advmt. Sci. **64**, 83 (1894).